PCCP

ROYAL SOCIETY OF CHEMISTRY

PAPER

View Article Online
View Journal | View Issue

Cite this: *Phys. Chem. Chem. Phys.*, 2021, **23**, 24413

Computational UV spectra for amorphous solids of small molecules

Austin M. Wallace and Ryan C. Fortenberry *

Received 16th July 2021,
Accepted 12th October 2021

DOI: 10.1039/d1cp03255k

rsc.li/pccp

Ices in the interstellar medium largely exist as amorphous solids composed of small molecules including ammonia, water, and carbon dioxide. Describing gas-phase molecules can be readily accomplished with current high-level quantum chemical calculations with the description of crystalline solids becoming more readily accomplished. Differently, amorphous solids require more novel approaches. The present work describes a method for generating amorphous structures and constructing electronic spectra through a combination of quantum chemical calculations and statistical mechanics. The structures are generated through a random positioning program and DFT methods, such as ωB97-XD and CAM-B3LYP. A Boltzmann distribution weights the excitations to compile a final spectrum from a sampling of molecular clusters. Three ice analogs are presented herein consisting of ammonia, carbon dioxide, and water. Ammonia and carbon dioxide provide semi-quantitative agreement with experiment for CAM-B3LYP/6-311++G(2d,2p) from 30 clusters of 8 molecules. Meanwhile, the amorphous water description improves when the sample size is increased in cluster size and count to as many as 105 clusters of 32 water molecules. The described methodology can produce highly comparative descriptions of electronic spectra for ice analogs and can be used to predict electronic spectra for other ice analogs.

Introduction

In cold interstellar regions and protoplanetary disks, amorphous solids exist due to the lack of energy required to produce crystalline solids. While specific molecular concentrations vary depending on the astrophysical environment, H_2O, H_2CO, N_2, CO, O_2, CO_2, H_2O_2, CH_4, and NH_3 are the primary constituents of grain mantles[1–5] that exist as amorphous solids in low temperatures. These amorphous solids can act as a surface upon which molecules accumulate and reaction pathways are accelerated. At temperatures around 10 K, most molecules—except H_2 and He—that collide with these ice analogs will stick to the surface.[6] More specifically, the surface of amorphous water has nanopores that have strong binding sites which allow adsorption of molecules, such as CO, permitting additional surface chemistry.[7,8] Due to increased flexibility, amorphous solids can behave as superior catalysts compared to their corresponding crystalline solid form.[7] Consequently, interstellar amorphous solids provide an environment for bringing molecules together and, subsequently, increasing their reactivity.

Additionally, amorphous solids can exist as ices and provide the material for forming larger molecules independently. Ultraviolet photolysis of ice analogs consisting of H_2O, CH_3, NH_3 and CO ultimately produces H_2CO_3, CO_2, CH_4, HCO and more complex molecules in simulated interstellar environments.[9–12] These products and other similar small molecules containing carbon atoms are likely precursors for forming larger organic and biologically relevant molecules in the interstellar medium (ISM).[6,9,13–19] Some of these compounds include glycine, alanine, and serine[20] with reaction pathways explored computationally.[21] Furthermore, previous theoretical and laboratory work shows that methane, ethylene, and acetylene ices can undergo radical reactions to produce larger alkanes.[22] Therefore, better ice analog characterization can lead to increased understanding of extraterrestrial environments in which organic residues form.

While many computational approaches exist for describing amorphous solids with molecular dynamics and machine learning,[23–26] few approaches attempt to use higher-levels of theory, such as density functional theory (DFT), to describe amorphous solids due to the high computational costs. Attempts at combining DFT and machine learning have produced favorable results for describing *ta*-C surfaces;[27] however, a gap exists in the literature regarding the description of electronic spectra of small molecule amorphous solids potentially present in the ISM. Other computational descriptions of ices have utilized B3LYP/6-31+G** with up to 12 water molecules and implicit solvent effects to describe water as an ice environment for simulating interactions between ammonia and formaldehyde.[28] Chen and Woon conclude that increasing the number of water molecules in the clusters seems to produce

Department of Chemistry & Biochemistry, University of Mississippi, University, Mississippi 38677-1848, USA. E-mail: r410@olemiss.edu; Tel: +1-662-915-1687

infrared modes that start converging in value with observations.[28] Other approaches with DFT investigate interactions with water ices with good agreement to experimental results.[29,30] Thus, DFT appears predictive for interstellar-like clusters in the infrared region.

Previous research on ices in interstellar regions primarily focuses on vibrational spectroscopy in the infrared region[31–34] with less investigation into electronic spectroscopy within the ultraviolet light region.[35,36] Infrared spectroscopy of amorphous CO_2 ices has shown that IR can detect mixtures of CO_2 with other small molecules and discern between ice and gas phase through attention to minor details.[37,38] While water in the gas phase has its first vertical excitation at about 7.5 eV, the amorphous solid is significantly higher in energy due to less favorable interactions with adjacent water molecules from the excited state's smaller dipole moment.[36] Due to ionization limits, each ice has a specific upper-bound energy for the observable electronically excited states before the energy changes the ice itself. As such, electronic excited states confined to a region below the ionization limit provides a region for comparing computation and experiment. In order to provide a computational description of the amorphous solids of ammonia, carbon dioxide, and water, the present work describes a method for generating these solids computationally and comparing the computed electronic spectroscopic data with experiment in the literature.[35] The generation of molecular structures uses randomization, and the optimizations and electronically excited states are calculated using DFT. After generating clusters of each of these molecules, the use of DFT for molecular optimizations and electronic spectroscopy in the current work aims to provide electronic spectral characterization for small molecule amorphous solids with application to elucidating the behavior of interstellar ices both in the laboratory and potentially even in astrophysical environments.

Computational methods and approach

Amorphous solids are computationally generated through a randomization program written in Python3. The program relies on two main parameters: number of clusters and number of molecules per cluster. After building the clusters and running optimization and electronic excitation calculations, spectroscopic data is extracted and weighted according to a Boltzmann distribution of the clusters' energies. The final output is a normalized spectrum based on combining all the clusters' data.

Prior to using the program, the desired molecule is optimized as a monomer. In the present work, ammonia, water, and carbon dioxide monomers are optimized with ωB97-XD/6-31G(d) through Gaussian16.[39–41] The optimized molecular geometry and cluster parameters, such as number of molecules in the system, number of clusters, and size of the box, are then input into the program. Additionally, differing geometries can be used with specific ratios to construct mixtures. Regardless of the parameters, each molecule in the cluster starts at the origin and undergoes randomized rotations and displacements according to values generated by the Mersenne Twister series,[42] which acts as a pseudorandom number generator. The random rotations occur in three planes. Then, the molecules are displaced by a randomly generated three-dimensional vector. In order to ensure that the molecular geometries do not overlap in the cluster—causing errors in the optimization calculations—the program checks the distance between each of the monomers in the system and the newly added monomer. If the distance is too small, the molecule undergoes the randomization process again. This cycle continues until the system contains the specified number of molecules. Upon completion, the program constructs Gaussian16 geometry optimization input files with Cartesian coordinates and frozen internal coordinates of bond length and bond angles within the individual molecules themselves.

The process described above is conducted for as many clusters as the user specifies. Next, each optimization calculation runs with ωB97-XD/6-31G(d) until the constrained molecular internal coordinates cause the calculation to fail to converge; however, this optimizes the distance between the molecules providing a better guess as to the preferred arrangement of the molecules. The last molecular geometry is extracted and placed into another Gaussian16 input file without freezing internal molecular coordinates in order to calculate the optimized geometry and harmonic frequency zero-point energy for the cluster. This two step process accelerates the optimization process and avoids nearly all imaginary frequencies. Then, the optimized geometries undergo time-dependent density functional theory (TD-DFT) electronic excitation calculations. Notably, the current work uses the optimized structures as a reference geometry for the exploration of different functionals and basis sets. The methods include B3LYP,[43] PBE0,[44] ωB97-XD,[41] CAM-B3LYP,[45] and B97D3.[46] The basis sets include 6-311G(d,p) and 6-311++G(2d,2p).[47,48]

After the optimizations finish, the program uses a Boltzmann distribution from the relative energies to acquire a scaling factor. The scaling factor is used to weight the contributions of each cluster's excitations oscillator strengths, which approximates Beer's Law. Additionally, the temperature parameter is set by the user to match the energy levels of the environment. For ammonia, water, and carbon dioxide, the temperature is calculated through converting the binding energies of the dimers into units of temperature. These binding energies come from optimizing the dimers with ωB97-XD/6-31G(d) and subtracting the energy from twice the monomer energy. From the Boltzmann distribution, the more stable clusters will contribute more to the overall spectrum than the less stable structures. The program then compiles the excitations into one file for a sub-processed artificial spectrum broadening program that uses the Gaussian line shape procedure with a full width at half maximum height (FWHM) variable of 2 nm to produce a continuous function from the discretely calculated spectra. To ensure that the broadness is consistent across all spectra produced by the program, the FWHM is set to 2 nm arbitrarily. Finally, a normalized spectrum (compared to the highest peak) of the oscillator strength is plotted as a function of energy.

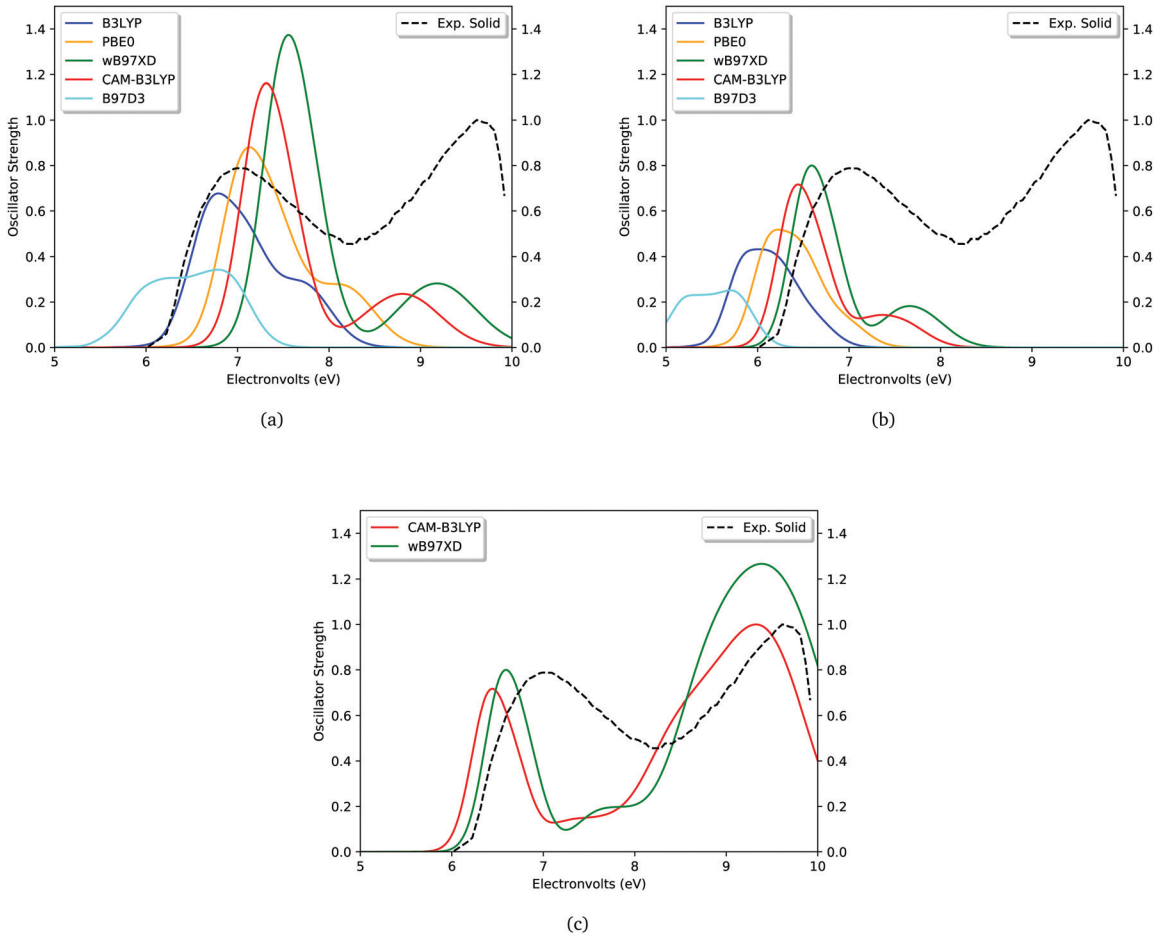

Fig. 1 VUV spectra for 30 clusters of 8 ammonia molecules normalized to the maximum oscillator strength in (c) for consistency, and the experimental plot[35] normalized to itself: (a) basis set: 6-311G(d,p) and states: 25; (b) basis set: 6-311++G(2d,2p) and states: 25; and, (c) basis set: 6-311++G(2d,2p) and states: 125.

In order to explore the capabilities of generating amorphous solid electronic spectra, four datasets are generated comprising of pure water, ammonia, or carbon dioxide. Since water has the fewest electrons of the listed molecules, two datasets of water are analyzed. One dataset comprises of 105 randomized clusters of 32 water molecules, while the other is 30 randomized clusters of 8 water molecules. The datasets for ammonia and carbon dioxide agree in size with the smaller water dataset of 30 randomized clusters of 8 molecules.

Results and discussion

Ammonia

A total of 30 octamer clusters of ammonia are generated with their spectra compared with experiment. The temperature for the Boltzmann distribution with ammonia is 1348 K corresponding to the binding energy of the dimerization which implies that all of the binding energy will be thermally released into the amorphous ice. This large assumption ultimately has little effect on the observed results due to the similarities of the excited state properties for the various molecular geometries. Initially, a dataset for several functionals are computed with the 6-311G(d,p) basis set with 25 electronic states to extend over 10 eV as shown in Fig. 1(a). All of the peaks are normalized to the oscillator strength of the maximum intensity peak from the CAM-B3LYP/6-311++G(2d,2p) spectrum from Fig. 1(c) to provide a standard normalization factor for comparing relative intensities of the functionals. The normalization emphasizes that the number of states calculated does not affect the raw intensities of an excited state calculation between CAM-B3LYP/6-311++G(2d,2p) displayed in Fig. 1(b and c).

The relative intensities are reported in Table 1. B3LYP appears to perform quite well with this basis set at describing the first peak shown from work by Mason *et al.*[35] while CAM-B3LYP, ωB97-XD, and PBE0 report higher in energy.

However, in order to better describe the hydrogen bonding interactions in the amorphous ammonia, diffuse orbitals and a larger basis set are computed. Fig. 1(b) utilizes the 6-311++G(2d,2p) basis set with the same functionals showing that all the hybrid functionals are lower in energy. Now, it appears as though CAM-B3LYP and ωB97-XD are matching the first peak the best. To extend the spectrum to 10 eV, a spectrum is built with CAM-B3LYP/6-311++G(2d,2p) and ωB97-XD/

Table 1 Tabulated format of the ammonia spectra displayed in Fig. 1. Experimental data comes from work produced by Mason *et al.*[35] All computational spectra are normalized to the maximum peak from CAM-B3LYP/6-311++G(2d,2p)

Method	Basis set	Excitation (eV)	Oscillator strength (normalized)
B3LYP	6-311G(d,p)	6.79	0.68
PBE0	6-311G(d,p)	7.13	0.88
wB97XD	6-311G(d,p)	7.56	1.37
wB97XD	6-311G(d,p)	9.18	0.28
CAM-B3LYP	6-311G(d,p)	7.32	1.16
CAM-B3LYP	6-311G(d,p)	8.80	0.24
B97D3	6-311G(d,p)	4.79	0.00
B97D3	6-311G(d,p)	6.30	0.31
B97D3	6-311G(d,p)	6.79	0.34
B3LYP	6-311++G(2d,2p)	6.02	0.43
PBE0	6-311++G(2d,2p)	6.23	0.52
wB97XD	6-311++G(2d,2p)	6.59	0.80
wB97XD	6-311++G(2d,2p)	7.66	0.18
wB97XD	6-311++G(2d,2p)	9.39	1.27
CAM-B3LYP	6-311++G(2d,2p)	6.44	0.72
CAM-B3LYP	6-311++G(2d,2p)	7.36	0.14
CAM-B3LYP	6-311++G(2d,2p)	9.32	1.00
B97D3	6-311++G(2d,2p)	5.70	0.25
Exp. solid		7.00	0.79
Exp. solid		8.33	0.48
Exp. solid		9.61	1.00

6-311++G(2d,2p) with 125 electronic states producing Fig. 1(c). The artificial spectrum matches with the experimental spectrum very well qualitatively and even semi-quantitatively. Both peaks of the CAM-B3LYP artificial spectrum match nicely with regards to relative oscillator strengths to the experimental solid; while ωB97-XD approximates the relative intensities with less accuracy. Therefore, 30 randomized clusters of 8 ammonia molecules with CAM-B3LYP/6-311++G(2d,2p) with 125 electronic excited states appears to effectively describe amorphous ammonia's UV spectrum.

Finally, the timings for the electronic excited states depend heavily on the number of states and the basis set size. The best results from the CAM-B3LYP and ωB97-XD with 6-311++G(2d,2p) and 125 states take an average of 13.20 and 13.56 hours, respectively, on the local high-performance computing cluster. With the 6-311++G(2d,2p) basis set and 25 states, these functionals run for an average of 4.67 and 5.17 hours, a reduction in time cost of roughly one-third. Lastly, the quickest option for these two functionals with 6-311G(d,p) and 25 states required 1.02 and 1.16 hours, which is relatively fast but produces the worst results. Thus, CAM-B3LYP finishes slightly faster than ωB97-XD and provides closer energies and relative intensities when utilizing larger basis sets and number of states.

Carbon dioxide

Amorphous carbon dioxide is simulated through the creation of 30 randomized clusters of eight carbon dioxide molecules. Since carbon dioxide interacts with itself much less than ammonia due to the lack of hydrogen bonding, the binding energy from the dimerization yields a lower temperature of 457 K for the Boltzmann distribution. Spectra from several functionals with 6-311G(d,p) are displayed in Fig. 2(a). Once again, the two functionals that match experiment the best are CAM-B3LYP and ωB97-XD; both predict a smaller peak at around 9 eV and a larger peak just over 10 eV. However, the relative oscillator strengths do not match well. B3LYP and B97D3 both have a major peak lower in energy than experiment and do not display two peaks with this basis set. Finally, PBE0 has two peaks that are of nearly equal strength. Therefore, only CAM-B3LYP and ωB97-XD appear to perform decently with this basis set.

In order to improve the possible physical representation, the basis set is increased to 6-311++G(2d,2p). While no hydrogen bonding exists in the carbon dioxide clusters, the oxygen and carbon atoms do benefit from extra d and p orbitals. The effects of the basis set are apparent as shown in Fig. 2(b). In order to cover the energy range of the experiment, 50 electronic states for each functional are calculated. While PBE0 aligns closer in energy to the experiment with this basis set, the qualitative description has a large shoulder. This shoulder is merged into the major peak due to the artificial spectrum broadener; however, the height for the peak is still too large. For both of

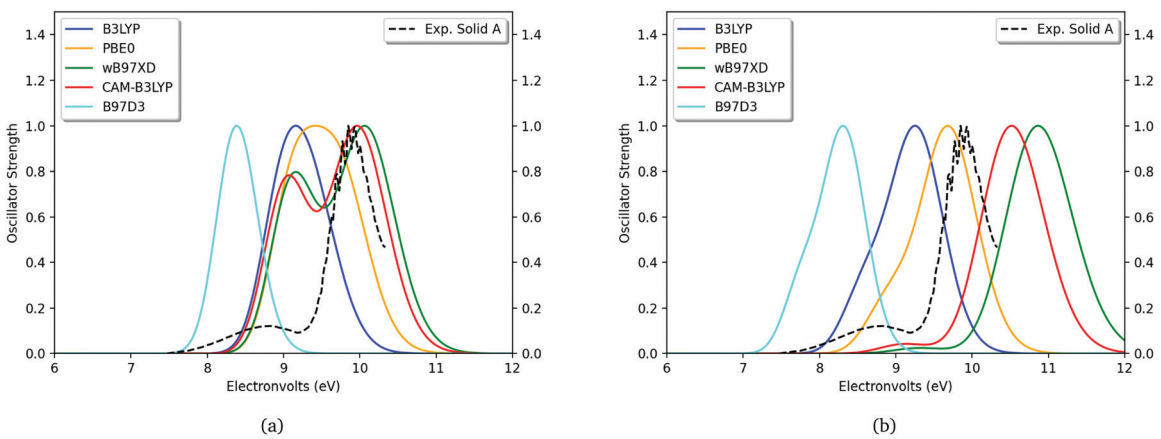

Fig. 2 VUV spectra for 30 clusters of 8 carbon dioxide molecules normalized to the maximum oscillator strength of each functional, and the experimental solid carbon dioxide plot[35] normalized to itself: (a) basis set: 6-311G(d,p) and states: 25; and (b) basis set: 6-311++G(2d,2p) and states: 50.

the predictive peaks in CAM-B3LYP and ωB97-XD, the excitation energies are higher than experiment. However, the curves for CAM-B3LYP and ωB97-XD match qualitatively well with experiment through a small peak separated by a much larger peak over 1 eV away. Thus, the CAM-B3LYP and ωB97-XD functionals describe amorphous carbon dioxide the effectively but not quite as well as they did with ammonia (Table 2).

Water

Two datasets of water are generated at varying cluster sizes to compare the results with each other. The larger dataset, 105 randomized clusters of 32 water molecules, should better approximate the reality of amorphous water; however, the objective is to determine if a smaller dataset, such as 30 randomized clusters of 8 water molecules, can make an equally valid approximation.

First, a dataset of 30 clusters with eight water molecules is generated to investigate with the same functionals listed above. Fig. 3(a) displays the 30 clusters of 8 water molecules for several functionals with 6-311G(d,p). From this water dataset, B3LYP

Table 2 Tabulated format of the carbon dioxide spectra displayed in Fig. 2. Experimental data comes from work produced by Mason *et al.*[35]

Method	Basis set	Excitation (eV)	Oscillator strength (normalized)
B3LYP	6-311G(d,p)	9.16	1.00
PBE0	6-311G(d,p)	9.42	1.00
wB97XD	6-311G(d,p)	9.16	0.80
wB97XD	6-311G(d,p)	10.06	1.00
CAM-B3LYP	6-311G(d,p)	9.07	0.78
CAM-B3LYP	6-311G(d,p)	9.97	1.00
B97D3	6-311G(d,p)	8.39	1.00
B3LYP	6-311++G(2d,2p)	9.25	1.00
PBE0	6-311++G(2d,2p)	9.68	1.00
wB97XD	6-311++G(2d,2p)	9.33	0.02
wB97XD	6-311++G(2d,2p)	10.86	1.00
CAM-B3LYP	6-311++G(2d,2p)	9.14	0.04
CAM-B3LYP	6-311++G(2d,2p)	10.52	1.00
B97D3	6-311++G(2d,2p)	8.31	1.00
Exp. solid		8.83	0.12
Exp. solid		9.63	0.60
Exp. solid		9.70	0.79
Exp. solid		9.77	0.93
Exp. solid		9.85	1.00
Exp. solid		9.93	1.00
Exp. solid		10.00	0.91

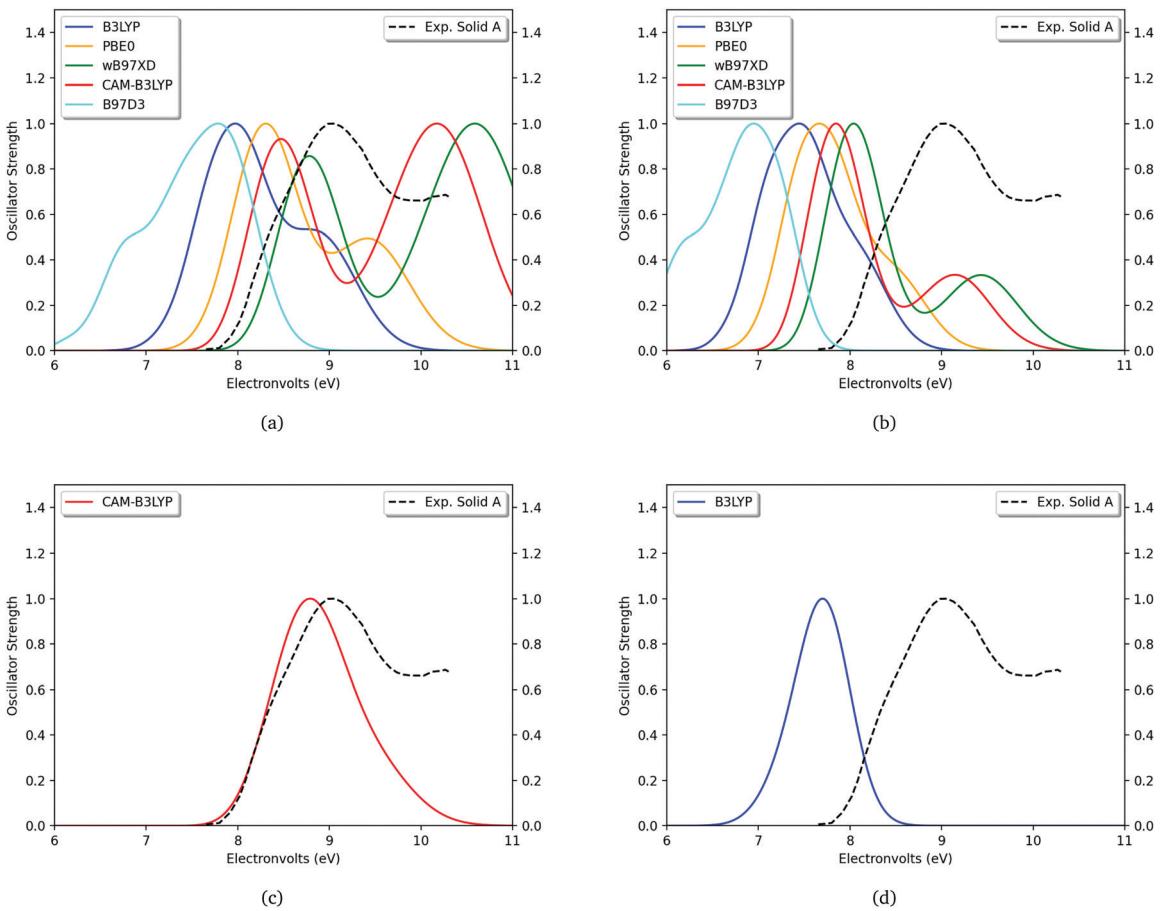

Fig. 3 VUV spectra for 30 clusters of 8 waters (a and b) and 105 cluster of 32 waters (c and d) compared with experiment.[35] All plots are normalized to themselves: (a) basis set: 6-311G(d,p) and states: 25; (b) basis set: 6-311++G(2d,2p) and states: 25; (c) basis set: 6-311G(d,p) and states: 50; and, (d) basis set: 6-311G(d,p) and states: 25.

Table 3 Tabulated format of the water spectra displayed in Fig. 3(a and b). Experimental data comes from work produced by Mason *et al.*[35]

Method	Basis set	Excitation (eV)	Oscillator strength (normalized)
B3LYP	6-311G(d,p)	7.98	1.00
B3LYP	6-311G(d,p)	8.76	0.56
PBE0	6-311G(d,p)	8.31	1.00
PBE0	6-311G(d,p)	9.42	0.51
wB97XD	6-311G(d,p)	8.79	0.86
wB97XD	6-311G(d,p)	10.61	1.00
CAM-B3LYP	6-311G(d,p)	8.48	0.96
CAM-B3LYP	6-311G(d,p)	10.19	1.00
B97D3	6-311G(d,p)	6.82	0.49
B97D3	6-311G(d,p)	7.81	1.00
B3LYP	6-311++G(2d,2p)	7.48	1.00
PBE0	6-311++G(2d,2p)	7.68	1.00
wB97XD	6-311++G(2d,2p)	8.05	1.00
wB97XD	6-311++G(2d,2p)	9.43	0.32
CAM-B3LYP	6-311++G(2d,2p)	7.86	1.00
CAM-B3LYP	6-311++G(2d,2p)	9.15	0.32
B97D3	6-311++G(2d,2p)	6.21	0.49
B97D3	6-311++G(2d,2p)	6.97	1.00

and PBE0 appear to perform the best qualitatively for water, while CAM-B3LYP and ωB97-XD predict a larger secondary peak that appears to be beyond the energy range of the experiment. With a larger basis set in Fig. 3(b), the functionals produce peaks lower in energy than experiment. While all of functionals report lower excitation energies than experiment, CAM-B3LYP and ωB97-XD (Table 3) report the closest values along with a secondary small peak as they did with ammonia. While these qualitative descriptions are in decent agreement with experiment at the cluster size of 8 water molecules, the energy and oscillator strength differences between the major peaks and experiment could be improved. The inaccuracy could be due to the small molecular weight of the water molecules and the hydrogen bonding not being fully represented.

Upon increasing the number of molecules from 8 to 32 in a cluster and the amount of clusters from 30 to 105, the spectrum is slightly lower in energy than the experimental values as in Fig. 3(c). CAM-B3LYP with 6-311G(d,p) and 50 states matches the experimental spectrum. Alternatively, B3LYP with 6-311G(d,p) and 25 states as in Fig. 3(d) displays a lower energy prediction as well, albeit not as strong. Regardless, both of these spectra support the notion that a dataset with more clusters and more molecules in each cluster better represents reality even with a smaller basis set.

To compare timings of the two datasets, the clusters with eight water molecules took an average of 0.51 hours for B3LYP/6-311G(d,p), whereas the 32 water molecule clusters averaged 15.83 hours for the same method, basis set and number of states. Additionally, the CAM-B3LYP/6-311G(d,p) with 25 states for the smaller clusters takes an average of 2.45 hours, while the much more accurate results with same method and basis set with 50 states takes an average of 31.46 hours per TD-DFT calculation. Clearly, the larger water cluster produces better results with the CAM-B3LYP/6-311G(d,p) and 50 states than the CAM-B3LYP/6-311++G(2d,2p) and 25 states; however, the cost is much higher but nowhere near prohibitively so.

The datasets presented above indicate that CAM-B3LYP is the best functional because it produces the best qualitative and semi-quantitative agreement with experiment. Due to the usage of DFT, no exact numerical predictions for the peak maximums are expected; however, the water example of increasing the cluster size from 8 to 32 molecules shows that larger clusters can drastically improve the accuracy of the numerical predictions. Furthermore, the number of states required to build a spectrum over a desired region will grow with increasing cluster sizes, atomic numbers of elements, and basis sets due to the increased number of molecular orbitals contributing to the electronic excited state calculations. As such and based on the present results, applying this method to amorphous solids without comparable experimental data should aim to have $n >= 8$ for the number of molecules in the clusters and use a basis set size of at least 6-311G(d,p). Future work will continue to refine this approach, but the present methodology serves as an initial means of predicting such spectra. Ultimately, the qualitative predictions for unknown molecular spectra should be used to guide experiment.

Conclusions

Ultimately, the methodology implemented herein utilizing a randomization program along with DFT calculations can produce predictive electronic spectrum descriptions for amorphous ices in the ISM or for laboratory analogues based on the present benchmarks for H_2, NH_3, and CO_2. The usage of a randomization procedure for generating arbitrary input geometries and a Boltzmann distribution to weight the excitations yields high qualitative, and even semi-quantitative, agreement with experiment for small molecule amorphous solid electronic spectra. Overall, the best functionals for this application are CAM-B3LYP and ωB97-XD because both yield high qualitative agreement with experimental values. While increasing the basis set size on ammonia and carbon dioxide produces better results, water requires additional water molecules and larger number of clusters to resemble reality better, even with a smaller basis set. Regardless, the solid correlation with experiment in the UV region provides evidence for these clusters mimicking amorphous solids as ice and that increasing cluster size improves the description. Therefore, the method described in this work effectively characterizes ice analogues through the usage of DFT and should be able to do so for other ices. Mixtures of molecules in the ices are, naturally, a next step and will be explored in future work.

Conflicts of interest

There are no conflicts to declare.

Acknowledgements

This work was supported by NSF Grant OIA-1757220, NASA Grant NNX17AH15G, and Startup Funds provided by the

University of Mississippi. The computing resources were provided by the Mississippi Center for Supercomputing Research. Additionally, AMW wishes to acknowledge support from the Barry Goldwater Scholarship and Excellence in Education Foundation. The codebase for generating the amorphous solid clusters can be found through the following link: https://github.com/Awallace3/ice_analog_spectra_generator.git.

Notes and references

1 A. G. G. M. Tielens and W. Hagen, *Astron. Astrophys.*, 1982, **114**, 245–260.
2 E. L. Gibb, D. C. B. Whittet, A. C. A. Boogert and A. G. G. M. Tielens, *Astrophys. J., Suppl. Ser.*, 2004, **151**, 35–73.
3 K. I. Öberg, A. C. A. Boogert, K. M. Pontoppidan, S. van den Broek, E. F. van Dishoeck, S. Bottinelli, G. A. Blake and N. J. Evans, *Astrophys. J.*, 2011, **740**, 109.
4 A. A. Boogert, P. A. Gerakines and D. C. Whittet, *Annu. Rev. Astron. Astrophys.*, 2015, **53**, 541–581.
5 K. Hiraoka, T. Miyagoshi, T. Takayama, K. Yamamoto and Y. Kihara, *Astrophys. J.*, 1998, **498**, 710–715.
6 R. Martín-Doménech, K. I. Öberg and M. Rajappan, *Astrophys. J.*, 2020, **894**, 98.
7 L. J. Karssemeijer, S. Ioppolo, M. C. van Hemert, A. van der Avoird, M. A. Allodi, G. A. Blake and H. M. Cuppen, *Astrophys. J.*, 2013, **781**, 16.
8 M. P. Collings, J. W. Dever, H. J. Fraser, M. R. S. McCoustra and D. A. Williams, *Astrophys. J.*, 2003, **583**, 1058–1062.
9 L. Allamandola, S. Sandford and G. Valero, *Icarus*, 1988, **76**, 225–252.
10 L. J. Allamandola, M. P. Bernstein, S. A. Sandford and R. L. Walker, *Composition and Origin of Cometary Materials*, Dordrecht, 1999, pp. 219–232.
11 P. Gerakines, W. Schutte and P. Ehrenfreund, *Astron. Astrophys.*, 1996, **312**, 289–305.
12 R. Hudson and M. Moore, *Icarus*, 1999, **140**, 451–461.
13 M. Moore and R. Khanna, *Spectrochim. Acta, Part A*, 1991, **47**, 255–262.
14 S. Ioppolo, Z. Kanuchová, R. L. James, A. Dawes, A. Ryabov, J. Dezalay, N. C. Jones, S. V. Hoffmann, N. J. Mason and G. Strazzulla, *Astron. Astrophys.*, 2021, **646**, A172.
15 R. I. Kaiser, S. Maity and B. M. Jones, *Angew. Chem., Int. Ed.*, 2015, **54**, 195–200.
16 K. I. Öberg, *Chem. Rev.*, 2016, **116**, 9631–9663.
17 K. K. Singh, P. Tandon, R. Kumar, A. Misra, Shivani, M. Yadav, A. Ahmad and M. K. Chaudhary, *Mon. Not. R. Astron. Soc.*, 2021, **506**(2), 2059–2065.
18 G. Fedoseev, K.-J. Chuang, E. F. van Dishoeck, S. Ioppolo and H. Linnartz, *Mon. Not. R. Astron. Soc.*, 2016, **460**, 4297–4309.
19 E. Herbst and E. F. van Dishoeck, *Annu. Rev. Astron. Astrophys.*, 2009, **47**, 427–480.
20 M. P. Bernstein, J. P. Dworkin, S. A. Sandford, G. W. Cooper and L. J. Allamandola, *Nature*, 2002, **416**, 401–403.
21 D. E. Woon, *Astrophys. J.*, 2002, **571**, L177–L180.
22 R. I. Kaiser and K. Roessler, *Astrophys. J.*, 1998, **503**, 959–975.
23 V. L. Deringer, N. Bernstein, A. P. Bartók, M. J. Cliffe, R. N. Kerber, L. E. Marbella, C. P. Grey, S. R. Elliott and G. Csányi, *J. Phys. Chem. Lett.*, 2018, **9**, 2879–2885.
24 G. C. Sosso, V. L. Deringer, S. R. Elliott and G. Csányi, *Mol. Simul.*, 2018, **44**, 866–880.
25 J. Mavračić, F. C. Mocanu, V. L. Deringer, G. Csányi and S. R. Elliott, *J. Phys. Chem. Lett.*, 2018, **9**, 2985–2990.
26 C. Arasa, M. C. van Hemert, E. F. van Dishoeck and G. J. Kroes, *J. Phys. Chem. A*, 2013, **117**, 7064–7074.
27 V. L. Deringer, M. A. Caro, R. Jana, A. Aarva, S. R. Elliott, T. Laurila, G. Csányi and L. Pastewka, *Chem. Mater.*, 2018, **30**, 7438–7445.
28 L. Chen and D. E. Woon, *J. Phys. Chem. A*, 2011, **115**, 5166–5183.
29 E. Escamilla-Roa and C. I. Sainz-Díaz, *J. Phys. Chem. C*, 2014, **118**, 3554–3563.
30 G. Bovolenta, S. Bovino, E. Vöhringer-Martinez, D. A. Saez, T. Grassi and S. Vogt-Geisse, *Mol. Astrophys.*, 2020, **21**, 100095.
31 B. M. Giuliano, R. M. Escribano, R. Martín-Doménech, E. Dartois and G. M. Muñoz Caro, *Astron. Astrophys.*, 2014, **565**, A108.
32 S. Bottinelli, A. C. A. Boogert, J. Bouwman, M. Beckwith, E. F. van Dishoeck, K. I. Öberg, K. M. Pontoppidan, H. Linnartz, G. A. Blake, N. J. Evans and F. Lahuis, *Astrophys. J.*, 2010, **718**, 1100–1117.
33 J. Bouwman, W. Ludwig, Z. Awad, K. I. Öberg, G. W. Fuchs, E. F. van Dishoeck and H. Linnartz, *Astron. Astrophys.*, 2007, **476**, 995–1003.
34 J. S. Holt, D. Sadoskas and C. J. Pursell, *J. Chem. Phys.*, 2004, **120**, 7153–7157.
35 N. J. Mason, A. Dawes, P. D. Holtom, R. J. Mukerji, M. P. Davis, B. Sivaraman, R. I. Kaiser, S. V. Hoffmann and D. A. Shaw, *Faraday Discuss.*, 2006, **133**, 311–329.
36 E. F. van Dishoeck, E. Herbst and D. A. Neufeld, *Chem. Rev.*, 2013, **113**, 9043–9085.
37 I. R. Cooke, E. C. Fayolle and K. I. Öberg, *Astrophys. J.*, 2016, **832**, 5.
38 P. A. Gerakines and R. L. Hudson, *Astrophys. J.*, 2015, **808**, L40.
39 M. J. Frisch, G. W. Trucks, H. B. Schlegel, G. E. Scuseria, M. A. Robb, J. R. Cheeseman, G. Scalmani, V. Barone, G. A. Petersson, H. Nakatsuji, X. Li, M. Caricato, A. V. Marenich, J. Bloino, B. G. Janesko, R. Gomperts, B. Mennucci, H. P. Hratchian, J. V. Ortiz, A. F. Izmaylov, J. L. Sonnenberg, D. Williams-Young, F. Ding, F. Lipparini, F. Egidi, J. Goings, B. Peng, A. Petrone, T. Henderson, D. Ranasinghe, V. G. Zakrzewski, J. Gao, N. Rega, G. Zheng, W. Liang, M. Hada, M. Ehara, K. Toyota, R. Fukuda, J. Hasegawa, M. Ishida, T. Nakajima, Y. Honda, O. Kitao, H. Nakai, T. Vreven, K. Throssell, J. A. Montgomery, Jr., J. E. Peralta, F. Ogliaro, M. J. Bearpark, J. J. Heyd, E. N. Brothers, K. N. Kudin, V. N. Staroverov, T. A. Keith, R. Kobayashi, J. Normand,

K. Raghavachari, A. P. Rendell, J. C. Burant, S. S. Iyengar, J. Tomasi, M. Cossi, J. M. Millam, M. Klene, C. Adamo, R. Cammi, J. W. Ochterski, R. L. Martin, K. Morokuma, O. Farkas, J. B. Foresman and D. J. Fox, *Gaussian 16 Revision c.01*, 2016, Gaussian Inc., Wallingford, CT.

40 W. J. Hehre, R. Ditchfield and J. A. Pople, *J. Chem. Phys.*, 1972, **56**, 2257–2261.

41 J.-D. Chai and M. Head-Gordon, *Phys. Chem. Chem. Phys.*, 2008, **10**, 6615–6620.

42 M. Matsumoto and T. Nishimura, *ACM Trans. Model. Comput. Simul.*, 1998, **8**, 3–30.

43 A. D. Becke, *J. Chem. Phys.*, 1993, **98**, 5648–5652.

44 C. Adamo and V. Barone, *J. Chem. Phys.*, 1999, **110**, 6158–6170.

45 T. Yanai, D. P. Tew and N. C. Handy, *Chem. Phys. Lett.*, 2004, **393**, 51–57.

46 S. Grimme, S. Ehrlich and L. Goerigk, *J. Comput. Chem.*, 2011, **32**, 1456–1465.

47 A. D. McLean and G. S. Chandler, *J. Chem. Phys.*, 1980, **72**, 5639–5648.

48 R. Krishnan, J. S. Binkley, R. Seeger and J. A. Pople, *J. Chem. Phys.*, 1980, **72**, 650–654.

